Detection of Spiral Waves in Video

Valentina N. Korzhova, Dmitry B. Goldgof
Dept. of Computer Science & Engineering
University of South Florida
Tampa, FL,33620-5399, USA
korzhova,goldgof@csee.usf.edu

Grigori M. Sisoev
School of Mathematics
University of Birmingham
Birmingham B15 2TT, UK
G.Sisoev@bham.ac.uk

Abstract

This paper presents novel video-based algorithms for detection and tracking of spiral waves in a spinning disk reactor. The algorithms are based on spiral wave model and their performance is compared with results predicted by the computational fluid dynamics algorithms for fluid flow. In each frame points on the top of waves are detected and a spiral model fitted to the points. Using experimental video data, the developed models and algorithms allow investigators to estimate the characteristics of wave regimes such as wavelength and inclination angles. Results computed from video data are compared with number predicted by the theoretical model.

1. Introduction

The flow of a liquid film over a rapidly rotating horizontal disk has many applications in chemical, medical, and engineering fields. Important applications are heat or mass exchanges between expended liquid and surrounded gas, blood oxygenation, and cooling devices. Different wave regimes have a strong influence on those processes.

The experimental investigations of flow over a spinning disk have attempted to measure the local maximum or mean of film thickness. Various mechanical, electrical, and optical techniques [1, 2, 3, 4] were attempted, but these techniques gave insufficient information for classifying wave regimes. Experimental observations [1, 2, 3, 4] have demonstrated that at a small flow-rate, a smooth film is formed, and at a moderately higher flow-rate, circumferential waves are formed. Further increase in flow rate leads to the appearance of spiral waves.

Theoretical explanation of experimental results has received increasing attention in resent published research. The waveless solutions, asymptotic and numerical, were investigated in [1]; their linear stability analysis was examined in [1, 5]. In recent papers [6] an evolution system of equations to model axisymmetric finite-amplitude waves

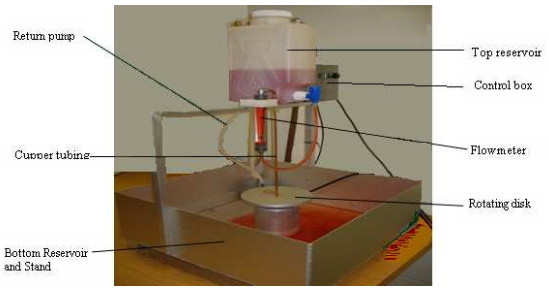

Figure 1. Experimental setup.

was derived and analyzed; this model is expended for non-axisymetric flows to explain the experimental results.

In the last decade, there has been significant work in image processing related to the motion analysis of non-rigid objects [7]. Most of the work has concentrated on articulated and elastic motion [8], but analysis of fluid-like motion was also attempted [9, 10]. Recently, work has begun in an effort to combine precise experimental setup, theoretical derivation, and basic image analysis techniques [3, 11].

The purpose of this paper is to develop algorithms for detection and tracking of a film flow over a spinning disk with the intention of detecting regimes of fluid flow with regard to differing conditions using a single camera system; to calculate fluid flow parameters; and to compare them with the solutions of the relevant mathematical models.

2. Data acquisition

The experimental set-up consists of a motor, aluminum flat/round stock, reservoir, tubing, brass adapters, flowmeter, copper tubing, aluminum control box, and return pump. The main characteristic of motor used is given by the turntable calibration. The image of the device is shown in Figure 1.

Measurements were performed in the following way. Water contained in a plastic container with an adjustment valve for the flow was drained through copper tubing at a constant flow starting rate r_0', which can be changed in the

0-7695-2521-0/06/$20.00 (c) 2006 IEEE

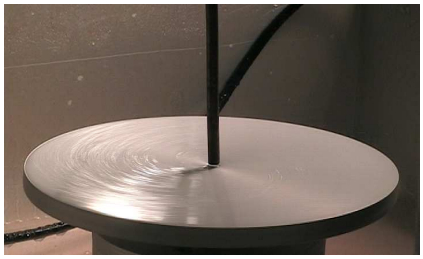

Figure 2. Rotating disk closeup

range 0.2-0.8 lpm (liter per minute). Liquid emerged from the nozzle as a free jet pouring out onto the center of a constantly rotating aluminum disk with a diameter of 200 mm. The rotational frequency of the disk was monitored by motor control. Water leaving the rotating disk is collected at the bottom reservoir and picked up to the top reservoir by a pump.

Ten videos were taken at different parameter settings (different arrangements of light and settings of the camera) using the portable camcorder Canon Optura 20, capable of capturing images at 30 fps (frame per second). Figure 2 shows a sample image of the liquid film that flows over a disk rotating with the angular velocity of 520 rpm (reverses per minute) and the flow rate of 0.8 lpm. The film surface is covered by spiral waves.

The pattern of 8×10 squares was used to calibrate the camera. Three hundred twenty points (corners of squares on the experimental pattern) were chosen in the Cartesian system coordinate with the origin in the center of the disk. The technique described in [12] was used for finding the intrinsic and extrinsic parameters of the camera.

3. Theoretical work

3.1. Evolution equations

A model derived in [6] is used in [13] with the addition of non-axisymmetric terms. A film of incompressible viscous liquid, of kinematic viscosity ν and density ρ, flows over a solid disc spinning with the angular velocity ω. A stationary cylindrical coordinate system, (r, ϕ, z), along with the velocity field (u_r, u_ϕ, u_z), are introduced to formulate the mathematical model describing the dynamics of the film bounded by the free surface ($z = h$) and underlying solid substrate ($z = 0$).

The flow is governed by the continuity equation, the Navier-Stokes equations, and an appropriate set of boundary conditions: no-slip and no–penetration at the disc surface, the kinematic boundary condition, shear and normal stress balances at the film surface. Detailed explanation of fluid flow modeling is outside the scope of this paper.

A localized version of equations derived in [13] allows for computation parameters of developing linear waves. The linearization leads to algebraic eigenvalue equation for dimensionless complex wave frequency that imaginary part, so-called amplification factor, indicates stability or instability of small perturbations. Most complicated perturbation corresponds to the wave with maximum amplification factor, and parameters of this wave are compared with experimental data. The corresponding instant local inclination of the spiral is $\tan\beta = \frac{1}{r}\frac{dr}{d\phi} = -\frac{n}{\alpha}$, where α and n are wave numbers along radial and azimuthal directions. Those numbers are compared with experimental measurements.

3.2. The spiral equations

Using the theory of spiral equations the following equations were utilized:

$$a_r = r''(t) = \omega^2 r - 8\pi f r'(t) - \frac{c}{2}\sin\beta r'^2(t),$$

$$a_s = v_s'(t) = 8\pi f(\omega r - v_s(t)) - \frac{c}{2}\cos\beta v_s^2(t),$$

$$\tan\beta = \frac{r'(t)}{v_s(t)} = (y_x' + \frac{y}{x})(1 + y_x' y_x) = \frac{1}{r}\frac{dr}{d\phi}, \quad (*)$$

$$\phi'(t) = \frac{r'(t)}{r(t)}\frac{1}{\sin\beta}, \frac{dr}{d\phi} = \frac{r(t)r'(t)}{v_s(t)},$$

$$\frac{d^2r}{d\phi^2} = \frac{r'^2 + r(t)r''(t)}{v_s(t)} - \frac{v_s'(t)r'(t)r(t)}{v_s^2(t)})\frac{1}{\phi'(t)},$$

$$r(0) = 0, r'(0) = r_0', r(T) = 100, v_s(0) = 0,$$

where a_r and a_s are accelerations along radius and perpendicular to radius, f and c are coefficients of spiral wave. It is clear that β is the angle between direction of the spiral and tangent. Figure 3 explains determination of $\phi(t)$ and $\tan\beta$.

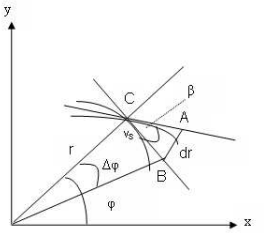

Figure 3. Determination of β and ϕ

The formula $\phi'(t) = \frac{r'(t)}{r(t)}\frac{1}{sin\beta}$ is not valid in the vicinity of $r(0) = 0$. Therefore, there is a need to use another model $\phi(t) = a \cdot t$, $a = \phi'(t)$ on the interval $(0, b)$ for small b.

Note that the second and third formulae for $\tan\beta$ in (*) can be used by image algorithms, since they do not depend on the time but only on geometric property of the spiral.

The approximate solution for this non-linear system is found using Euler's numerical method with decreasing steps of computation until approximate solutions are stabilized. In the case of water we have $8\pi f = 0.4\ mm^{-1}$, $c = 2\ mm^{-1}$, and $r_0' = \frac{3.8\cdot10^6}{285\cdot2\pi\cdot2.5\cdot3} \approx 280$ mm/s. Here ω is obtained from the respective graph for the reactor used, and $r'(0)$ is obtained from the experiment, in which 3.8×10^6 mm^3 is volume of a gallon of water, $285\ s$ is the time for the

water to run out of the respective capacity (see Figure 1), 2.5 mm is the radius of the tube, and 3 mm is the gap between the end of the tube and the disk surface.

3.3. Calibration camera accuracy

In order to extract metric information from 2D images the camera calibration method described in [12] is used. The relationship between a 2D point (X, Y) and its image projection (x, y) is given by

$$\begin{bmatrix} x \\ y \\ 1 \end{bmatrix} = \begin{bmatrix} s & \gamma & c_x \\ 0 & s & c_y \\ 0 & 0 & 1 \end{bmatrix} \cdot [r_1, r_2, t] \cdot [X, Y, 1]^T,$$

where $[r_1, r_2, t]$ are the extrinsic parameters, (c_x, c_y) is a principal point, $s = f/s_x = f/s_y$, f is the focal length in the pixels, s_x is a scale factor, and γ is the skewness of the image axes. In our case $s_x = 0.6$ mm and $s = f/s_x = 512$ mm. So, assuming that the absolute error $\triangle s < 1$ pixel, the relative error is $\triangle s/s < 0.001$.

Considering lens distortion of a camera with coefficients k_1 and k_2, and using the results from [12] that the standard relative deviations for estimates of k_1 and k_2 do not exceed 3-4%, it follows that $\frac{dr}{r} \approx \frac{dx}{x} + \frac{dy}{y} \leq 0.0026$. Similarly, in the case $R = \sqrt{X^2 + Y^2}$ we find $\frac{dR}{R} < \frac{dx}{x} + \frac{dy}{y} + \frac{ds}{s^2}\frac{1}{R} \leq 0.0026 + 0.000001 < 0.003$. These estimates of the errors were used for experimental estimation of the spiral inclination of the film flow as an ill-posed computational problem of differentiation [14].

4. Algorithms and results

The block-scheme of detecting the points on the waves and estimating the wave parameters is given in Figure 4.

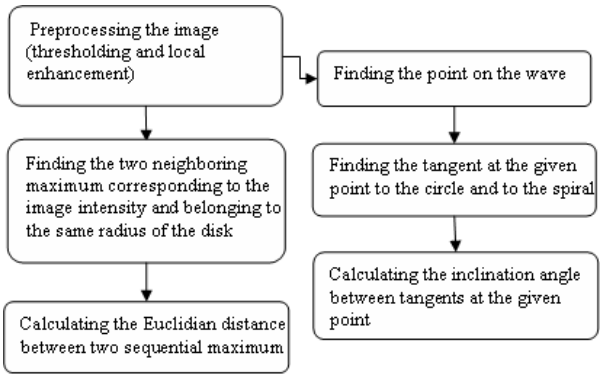

Figure 4. Block-scheme of detection waves and experimental calculations.

In order to detect the points on the waves the following sequence of operations is performed: the image scaling: the pixels with intensity I $>$ 220 are expanded to I + 10 and with I $\leq$ 220 to I - 20; the local histogram equalization; the average intensities are defined for 4 radii at an increment $\frac{1}{57}$ radian; the fifteen first maximums were found on the averaging radius lied in the enhancement window. The resulting image is shown in Figure 5.

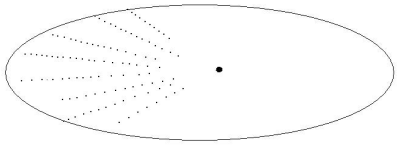

Figure 5. The detected points on the waves.

4.1. Estimation of inclination angles and wavelengths

Figure 3 shows the determination of an inclination angle β. The problem of estimation of β is ill-posed [14]. So, the so-called quasi-optimal method [14] to minimize an error of estimate under known error of initial data was used. The quasi-optimal step $d\phi = (\frac{4\epsilon}{R}\frac{R}{M_2})^{\frac{1}{2}}$ is $(\approx \frac{1}{40} radian)$, where $\frac{\epsilon}{R}$ is a relative error of camera calibration (≈ 0.003) and $M_2 = \max(\frac{r''(\phi)}{d\phi^2})$ is found from the spiral equations $(\frac{M_2}{R} \approx 17)$. An error produced by image processing was estimated as $2\sqrt{\frac{M_2}{M_1}\frac{R}{M_1}\frac{\epsilon}{R}}$ $(\approx \pm 9\%)$, where $M_1 = \max r'(\phi) \approx 800\ \frac{mm}{rad}$.

In order to calculate the radial wavelength l the difference between two neighboring waves, in radial direction, was calculated $(l = r_2 - r_1)$.

4.2. Comparison

The five videos with the sequence of ten frames of each of them for the flow rate of 0.8 lpm and the rotation of disk of 520 rpm were used for determination of the wavelength (W) (see Table 1). Average results of calculated (w_{ci}) and

Videos	The calculated wavelengths (centimeter)						
$n/radii$	4	5	6	7	8	9	10
1	.50	.41	.31	.29	.26	.24	.22
2	.46	.40	.30	.27	.23	.21	.20
3	.48	.39	.31	.25	.24	.22	.21
4	.43	.37	.27	.23	.22	.21	.19
5	.42	.36	.27	.23	.21	.21	.19

a)

$W/radii$	4	5	6	7	8	9	10
$Predicted$	.45	.39	.30	.26	.23	.22	.20
$Calculated$	.46	.40	.29	.25	.23	.22	.20

b)

Table 1. The calculated averaged wavelength a) of the sequence of ten frames, b) over five videos and theoretical wavelength.

theoretically predicted (w_{pi}) wavelengths are shown in Figure 6.

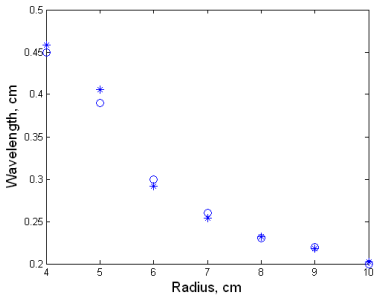

Figure 6. Dependence of wavelength on radius. Asterisks and x(s) correspond to experimental and theoretical, respectively.

It can be seen in Figure 6 that there is good correspondence between theoretical prediction of wavelengths and experimental data. The average relative error $(\frac{\sum_{i=1}^{n} \frac{|w_{ci}-w_{pi}|}{w_{ci}}}{n})$ is $\approx \pm 1\%$. In addition, as predicted, the wavelength decreases as radii increases.

The video of fluid flow over rotating disk of 520 rpm and the flow rate of 0.8 lpm was used to calculate the changes of wave inclinations $(|\beta(\phi + \Delta\phi) - \beta(\phi)|)$. The sequence of ten frames were processed to find the average change of inclination angles for radii in the range 4-10 cm. The changes of inclination angles $(\Delta\beta)$ are shown in the Table 2.

$\Delta\beta/radii$	4	5	6	7	8	9	10
$Predicted$	0	.08	.06	.04	.02	.01	.02
$Calculated$	0	.09	.08	.06	.05	.03	.01

Table 2. The inclination angle changes.

The experimental inclinational angle changes agree rather well with the results of the predicted inclinational angle changes. The average error is $\approx \pm 2\%$. In accordance with experimental observations and theoretical prediction, the inclination angle β decreases as radius grows.

5. Conclusion

This paper presents novel video-based algorithms for detection and tracking of spiral waves in a spinning disk reactor. In each frame points on the top of multiple waves are detected and a spiral model fitted to the points. Based on these computation the wavelength is estimated. In addition, the inclination angles between spirals and the respective circles and the radii between the center of a disk and points that lie on the front of curves in the direction of spinning disk are calculated using the so-called quasi-optimal method, which minimizes error of differentiation estimate under known error of initial data. Similar estimates are absent in literature. Results computed from video data are compared with number predicted by the theoretical model. In particular, the average computed wavelength is within 1% of the predicted values and a average error of inclination angle change computation is within 2%. The goal of this research to develop image-based fluid flow observation algorithms capable of computing fluid flow parameters and suitable for industrial inspection applications.

6. Acknowledgment

The authors acknowledge the financial support in part by the grant from the National Research Council, Collaboration in Basic Science and Engineering (COBASE) 2003 program.

References

[1] A.F. Charwat, R.E. Kelly, and C. Gazley, "The flow and stability of thin liquid films on a rotating disk", J. Fluid Mech 53(2), 227-255 (1972).

[2] A.I. Butuzov and I.I. Puhovoi, "On regimes of liquid film flows over a rotating surface", Journal of Engineering Physics 31(2), 217-224 (1976).

[3] W.P. Woods, The hydrodynamics of thin liquid films flowing over a rotating disc, Ph.D. thesis, University of Newcastle upon Tyne, UK (1995).

[4] G. Leneweit, K.G. Roesner, and R. Koehler, "Surface instabilities of thin liquid film flow on a rotating disk", Experiments in Fluids 26(1-2), 75-85 (1999).

[5] G.M. Sisoev and V.Y. Shkadov, "Flow stability of a film of viscous liquid on the surface of a rotating disc", Journal of Engineering Physics 52(6), 671-674 (1987).

[6] G.M. Sisoev, O.K. Matar, and C.J. Lawrence, "Axisymmetric wave regimes in viscous liquid film flow over a spinning disk", J. Fluid Mech 495, 385-411 (2003).

[7] C. Kambhamettu, D.B. Goldgof, D. Terzopoulos, and T. Huang, Computer Vision, Handbook of Pattern Recognition and Computer Vision, vol. 2 (11). Academic Press. (1994)

[8] D.B. Goldgof, H. Lee, and T. Huang, "Motion analysis of nonrigid surfaces", In: IEEE Conference on Computer Vision and Pattern Recognition, 899-904. Ann Arbor, Michigan, USA (1988).

[9] J. Zhong, T.S. Huang, and R.J. Adrian, "Salient structure analysis of fluid flow", Computer Vision and Pattern Recognition. Proceedings CVPR '94., 310-315 (1994).

[10] L. Zhou, C. Kambhamettu, D.B. Goldgof, K. Palaniappan, and A. Hasler, "Tracking nonrigid motion and structure from 2d satellite cloud images without correspondences", IEEE Transactions on PAMI 23, 1330-1336 (2001).

[11] S. Misra, M. Thomas, C. Kambhamettu, J. Kirby, F. Veron, and M. Brocchini, "Estimation of complex air-water interfaces from particle image velocimetry images", Experiments in Fluids (2006)

[12] Z. Zhang, "A flexible new technique for camera calibration", IEEE Transactions on PAMI 22, 1330-1334 (2000).

[13] G.M. Sisoev, Private communication.

[14] V.A. Morozov, "On Problem Differentiation and Experimental Information Approximation Algorithms", Computational Methods and Programming 14, Moscow Univ., 46-62 (1970).